Available online at www.sciencedirect.com

SCIENCE DIRECT®

Biochimica et Biophysica Acta 1616 (2003) 174–183

BIOCHIMICA ET BIOPHYSICA ACTA

BBA

www.bba-direct.com

Miscibility and phase behaviour of binary mixtures of *N*-palmitoylethanolamine and dipalmitoylphosphatidylcholine

Musti J. Swamy[a,*], M. Ramakrishnan[a], D. Marsh[b], U. Würz[b]

[a] *School of Chemistry, University of Hyderabad, Hyderabad 500 046, India*

[b] *Abteilung Spektroskopie, Max-Planck-Institut für biophysikalische Chemie, 37070 Göttingen, Germany*

Received 11 February 2003; received in revised form 12 August 2003; accepted 28 August 2003

Abstract

The content of *N*-acylethanolamines (NAEs) increases dramatically in cell membranes when the parent organism is subjected to injury or stress. This increase has been attributed to stress-combating mechanisms of the organism. In this study, a binary phase diagram of hydrated mixtures of *N*-palmitoylethanolamine (NP-E)—an endogenous ligand for the peripheral cannabinoid receptor (CB-2)—with dipalmitoylphosphatidylcholine (DPPC) is established by high-sensitivity differential scanning calorimetry (DSC). The structures of the phases involved were determined by using ^{31}P-NMR spectroscopy and low-angle X-ray scattering. DSC studies show that NP-E and DPPC mix well in the composition range DPPC/NP-E = 100:0 to 40:60 (mol/mol). At higher contents of NP-E, phase separation is indicated by the presence of additional transitions in the thermograms. Characterization of the structures formed by the mixtures with ^{31}P-NMR shows that, up to 80 mol% NP-E, DPPC remains in the lamellar phase. The low-angle X-ray diffraction data are also consistent with a lamellar gel-phase structure for DPPC/NP-E mixtures up to 60 mol% NP-E. Above 70 mol% NP-E, NP-E phase separates in the gel-phase region, while complete miscibility is observed in the fluid phase. These results provide a structural basis for understanding the membrane interactions of NAEs, which is necessary for understanding the mechanism of their putative stress-combating role in the parent organisms.

Keywords: *N*-Acylethanolamine; Differential scanning calorimetry; Low-angle X-ray diffraction; ^{31}P NMR; Lipid membrane; Phase diagram

1. Introduction

N-Acylethanolamines (NAEs) and *N*-acylphosphatidylethanolamines (NAPEs) are naturally occurring single-chain and three-chain membrane lipids, respectively, whose content in plant and animal tissues increases quite dramatically when the parent organism is subjected to stress or injury [1,2]. It was postulated that this increase could be part of a stress/injury-combatting mechanism of the organism. NAEs are produced in vivo by the enzymatic degradation of NAPEs, catalysed by a phospholipase-D type enzyme that is regulated by a signalling mechanism [3,4]. While NAPEs are negatively charged, NAEs are neutral. In the last decade, interest in NAEs was renewed with the discovery that anandamide (*N*-arachidonylethanolamine) and *N*-palmitoylethanolamine (NP-E) act as endogenous ligands for the type-I and type-II cannabinoid receptors, respectively, in mammals [5,6].

In addition to the ability of NP-E and anandamide to interact with cannabinoid receptors, NAEs also exhibit several other interesting biological properties. For example, anandamide has also been shown to inhibit sperm fertilizing capacity and gap-junction conductance [7,8], whereas *N*-oleoylethanolamine is a potent inhibitor of ceramidase [9]. Challenging cultured tobacco cells with xylanase (a fungal elicitor) leads to the secretion of *N*-myristoylethanolamine (NM-E) and *N*-lauroylethanolamine into the culture medium [10]. Further, NAEs are also of considerable interest be-

Abbreviations: NAE, *N*-acylethanolamine; NP-E, *N*-palmitoylethanolamine; NS-E, *N*-stearoylethanolamine; NM-E, *N*-myristoylethanolamine; NAPE, *N*-acylphosphatidylethanolamine; DPPC, dipalmitoylphosphatidylcholine; CB-2, peripheral cannabinoid receptor; DSC, differential scanning calorimetry; ^{31}P NMR, phosphorus 31-nuclear magnetic resonance; ESR, electron spin resonance; CSA, chemical shift anisotropy; EDTA, ethylenediaminetetraacetic acid; HEPES, *N*-(2-hydroxyethyl)piperazine-*N*′-2-ethanesulfonic acid; HBS, 10 mM HEPES buffer, containing 1 mM EDTA, pH 7.4

* Corresponding author. Tel.: +91-40-2301-1071; fax: +91-40-2301-2460/0145.

E-mail address: mjssc@uohyd.ernet.in (M.J. Swamy).

0005-2736/$ - see front matter © 2003 Elsevier B.V. All rights reserved.
doi:10.1016/j.bbamem.2003.08.008

cause of their pharmacological and medicinal properties as anti-inflammatory, anti-viral and anti-anaphylactic agents (reviewed in Ref. [1]).

While many studies have been focused on the identification of the cytoprotective abilities of NAEs and NAPEs, as well as on the characterization of their medical and pharmacological properties, studies aimed towards understanding the membrane physical properties of these lipids, such as their phase behavior and interaction with other membrane components, are comparatively scarce [11]. In order to understand structure-function relationships of these lipids, systematic studies of their physical properties and interaction with other membrane constituents are essential. Such studies can lead to an understanding of the role of these lipids within the cell membrane and may reveal mechanisms whereby they help the organism in combating stress. In earlier studies, Ambrosini et al. [12,13] investigated the interaction of several NAEs with dipalmitoylphosphatidylcholine (DPPC) multilamellar liposomes and also showed that NAEs can stabilize the bilayer structure against formation of the H_{II} phase. Additionally, Epps and Cardin [14] showed that increasing the concentration of *N*-oleoylethanolamine in DPPC vesicles leads to a decrease in the chain-melting phase transition temperature of the phospholipid. In previous studies, we have characterized the phase transitions of dry and hydrated forms of NAEs of even and odd chainlengths [15,16] and investigated the molecular packing and intermolecular interactions in crystals of NM-E by X-ray diffraction analysis [17].

The interaction of NP-E [CH_3-$(CH_2)_{14}$-(C=O)-NH-CH_2-CH_2-OH] with DPPC in hydrated mixtures was investigated in the present study by using differential scanning calorimetry (DSC). The binary temperature-composition phase diagram was constructed, and the structures of the phases formed were investigated by ^{31}P-NMR spectroscopy and low-angle X-ray diffraction measurements. The results obtained indicate that the two lipids mix well up to ca. 60 mol% of NP-E, whereas at higher mole fractions phase separation occurs.

2. Materials and methods

2.1. Materials

DPPC was obtained from Avanti Polar Lipids (Alabaster, AL, USA). Palmitic acid was from Sigma (St. Louis, MO, USA). Oxalyl chloride, HEPES and EDTA were obtained from Fluka (Buchs, Switzerland). NP-E was synthesized and characterized as described earlier [15].

2.2. Sample preparation

Samples for DSC were prepared by dissolving the two lipids in dichloromethane and mixing appropriate aliquots of the two solutions to give the desired mole ratio. The solvent was then evaporated by blowing dry nitrogen gas gently over the sample, and the final traces of solvent were removed by vacuum desiccation. The dry lipid mixture (ca. 2–4 mg) was hydrated with 500 μl of 10 mM HEPES buffer (pH 7.4) containing 1 mM EDTA at ca. 60 °C and then subjected to five cycles of freeze thawing.

Samples for phosphorus 31-nuclear magnetic resonance (^{31}P NMR) spectroscopy were prepared by codissolving 20–40 mg of the required lipid mixture (NP-E + DPPC) in dichloromethane, removing the solvent by rotary evaporation, and drying overnight under vacuum. The dry lipid was hydrated with 0.5 ml of 10 mM HEPES buffer, containing 1 mM EDTA, pH 7.4 (HBS) at approximately 10° above the chain-melting temperature of NP-E, and transferred to a 10-mm-diameter NMR tube. Samples were freeze-thawed five times, then pelleted in a bench-top centrifuge, and excess buffer was removed prior to measurement.

For X-ray diffraction measurements, either an aliquot of the samples prepared for NMR spectroscopy or a smaller sample prepared in an equivalent manner was transferred to a 1-mm-diameter, fine-wall glass capillary and centrifuged at 3000 rpm in a bench top centrifuge for ca. 5 min, and the excess supernatant was removed. The capillary was then flame-sealed.

2.3. DSC

DSC experiments were carried out on a Hart Scientific 4207 heat-flow differential scanning calorimeter, essentially as described earlier [18]. Samples, prepared as described above, were placed in 1.5-ml Hastelloy ampoules with screw-top lids and calorimetric scans were recorded at a rate of 10°/h (Celsius scale). An empty reference cell was used and baseline correction was made with a blank buffer sample.

2.4. X-ray diffraction

X-ray diffraction measurements were performed using a Kratky small-angle X-ray camera with a single-entrance slit of a width of 30 μm [19]. Compared with the range of scattering angles covered, the slit can be regarded as of infinite length, and the half-width of the beam (1.5×10^{-3} $Å^{-1}$) is negligible. Sample capillaries were mounted in a massive copper housing, which was thermostatted with a Peltier device. Temperature stability was better than 0.1 K. Nickel-filtered Cu K_α radiation ($\lambda = 0.154$ nm) was obtained from an AEG fine-focus tube, and diffracted intensity was recorded with a linear position-sensitive detector mounted on an extensive tube at a distance of 98.35 cm from the sample. To record data at higher scattering angles, the detector was repositioned in the vertical direction (which is orthogonal to the beam). Diffraction patterns are presented as scattering intensity that has not been corrected for the slit geometry.

2.5. ^{31}P NMR spectroscopy

Proton-dipolar decoupled ^{31}P-NMR spectra were recorded at a frequency of 121.5 MHz on a Bruker MSL-300 spectrometer operating in the Fourier transform mode. The $\pi/2$ pulse width was 11 μs, and recycle delays were always in excess of $5T_1$. The decoupling power was approximately 10–15 W, and the duty cycle of the gated decoupling was ca. 0.2%. Temperature was regulated by a thermostatted nitrogen gas-flow system.

3. Results

In the present study, the interaction between NP-E and DPPC, lipids of identical chainlength, has been characterized by DSC. The polymorphic structure of the mixtures was characterized from the unidimensional bilayer repeat distance (d_{100}) and the ^{31}P-chemical shift anisotropy (CSA), by using low-angle X-ray diffraction and ^{31}P NMR, respectively.

3.1. DSC

Heating and cooling thermograms of DPPC, NP-E and hydrated mixtures of these two lipids at different compositions are shown in Figs. 1 and 2, respectively. From Fig. 1A it can be seen that the pretransition and chain-melting transition of DPPC, observed at ca. 34.5 and 42 °C, respectively, are consistent with literature values [20]. The single transition observed for hydrated NP-E at around 80 °C (Fig. 1B), is also consistent with literature reports [15]. This high chain-melting phase transition temperature is most likely due to intermolecular hydrogen bonds between NP-E molecules, because NM-E and *N*-stearoylethanolamine (NS-E), which are homologous to this compound, exhibit extensive intermolecular hydrogen bonding networks in the crystalline state [17,21]. In the presence of 10 mol% NP-E, both the pretransition and the chain-melting transition of DPPC shift to higher temperatures with slight broadening. At 20 mol% NP-E, the pretransition disappears completely and the chain-melting transition is very considerably broadened. Broad, asymmetric endotherms are seen for samples containing 20–50 mol% of NP-E, and the shape of these changes with composition. At 60 mol% NP-E, only a single transition is seen, and this is sharper than the endotherms for samples in the 20–50 mol% NP-E composition range. The onset of the endotherm increases gradually in temperature with increasing NP-E content up to 60 mol%. Considerable changes occur in the phase behaviour of the DPPC/NP-E mixtures above 60 mol% NP-E. At 65 mol% NP-E, multiple endothermic peaks are seen and, most interestingly, the

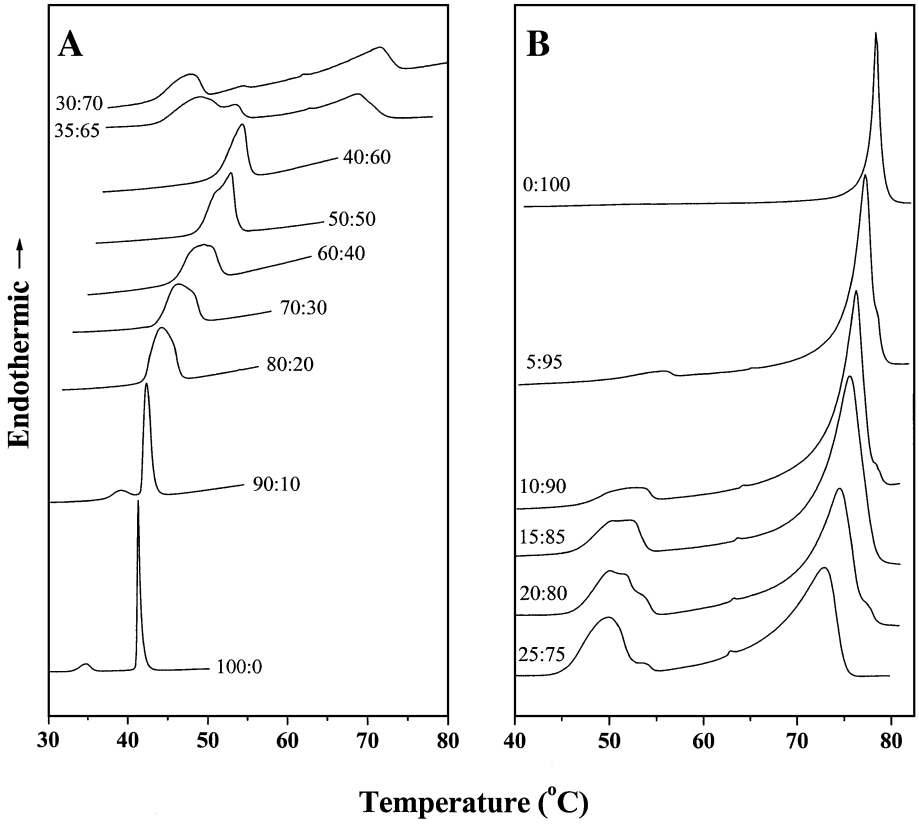

Fig. 1. Calorimetric heating scans of NP-E, DPPC and their mixtures at different compositions. Samples were dispersed in 10 mM HEPES, and 1 mM EDTA, pH 7.4. Scan rate: 10°/h (Celsius scale). The DPPC/NP-E mole ratio for each sample is indicated.

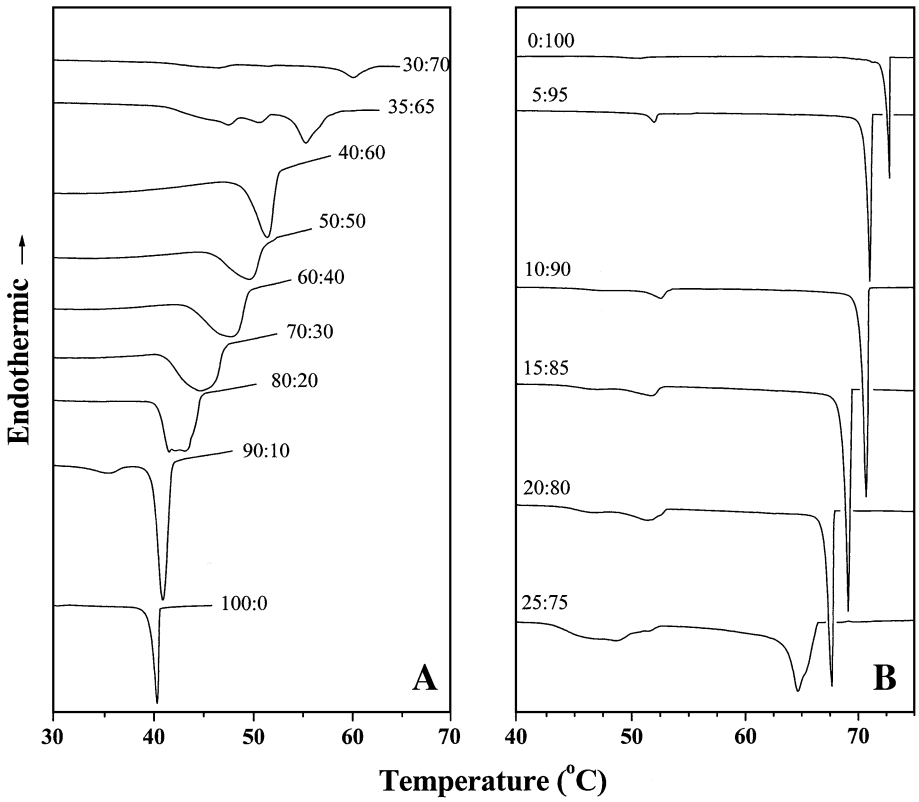

Fig. 2. Calorimetric cooling scans of NP-E, DPPC and their mixtures at different compositions. Samples were dispersed in 10 mM HEPES, and 1 mM EDTA, pH 7.4. Scan rate: 10°/h (Celsius scale). The DPPC/NP-E mole ratio for each sample is indicated.

onset temperature of the entire endotherm shifts to a lower temperature. Above 70 mol%, increase in the NP-E content results in only small increases in the onset temperature up to 90 mol% NP-E, and the overall shape of the endotherms remains rather constant. Above 90 mol% NP-E, the onset temperature increases rather steeply.

The corresponding DSC cooling scans are shown in Fig. 2A and B. The transitions corresponding to chain melting appear at several degrees below the corresponding heating transitions and are considerably sharper. The additional calorimetric peaks alluded to above for the mixtures containing >60 mol% NP-E are also seen in the cooling scans and appear at slightly lower temperatures than the corresponding transitions seen in the heating scans.

3.2. Binary phase diagram

Binary temperature-composition phase diagrams constructed from the heating and cooling thermograms presented in Figs. 1 and 2 are shown in Fig. 3A and B, respectively. The onset and completion temperatures of the entire endotherm (solid symbols) are plotted against NAPE content. The overall phase diagram appears qualitatively similar for both heating and cooling. Minor differences are seen which reflect the small hysteresis that is observed between the heating and cooling scans, especially for the major chain-melting event of the mixtures with higher contents of NP-E. Up to 60 mol% NP-E the two components appear to mix well, but above this composition range the thermograms become more complex in structure, suggesting partial immiscibility and possibly even multiple transitions, i.e., polymorphism. In this composition range, completion temperatures are plotted also for the two composite peaks at low temperature in Figs. 1 and 2. These are given by the open symbols in Fig. 3 and imply polymorphic behavior at high NAPE contents, as discussed later.

3.3. ^{31}P NMR

The broad-line proton-dipolar decoupled ^{31}P NMR spectra of mixtures of DPPC and NP-E are shown in Fig. 4, and values of the effective chemical shift anisotropies (CSA) obtained from the spectra shown in this figure are listed in Table 1. The three panels shown in Fig. 4 correspond to DPPC/NP-E (mol/mol) ratios of 2:1, 1:2 and 1:4, respectively. At 25 and 40 °C, corresponding to the gel phases, the spectra for all the three samples are broad, axially anisotropic powder patterns with a low-field shoulder and a high-field peak. The effective chemical shift anisotropies are in the range of $\Delta\sigma = -62.7$ to -71.2 ppm and are characteristic of a lamellar gel phase (Table 1). At higher temperatures, the spectra for the samples with DPPC/NP-E molar ratios of 2:1 and 1:2 are relatively sharp, axially anisotropic powder patterns with effective CSA values of $\Delta\sigma = -44.2$

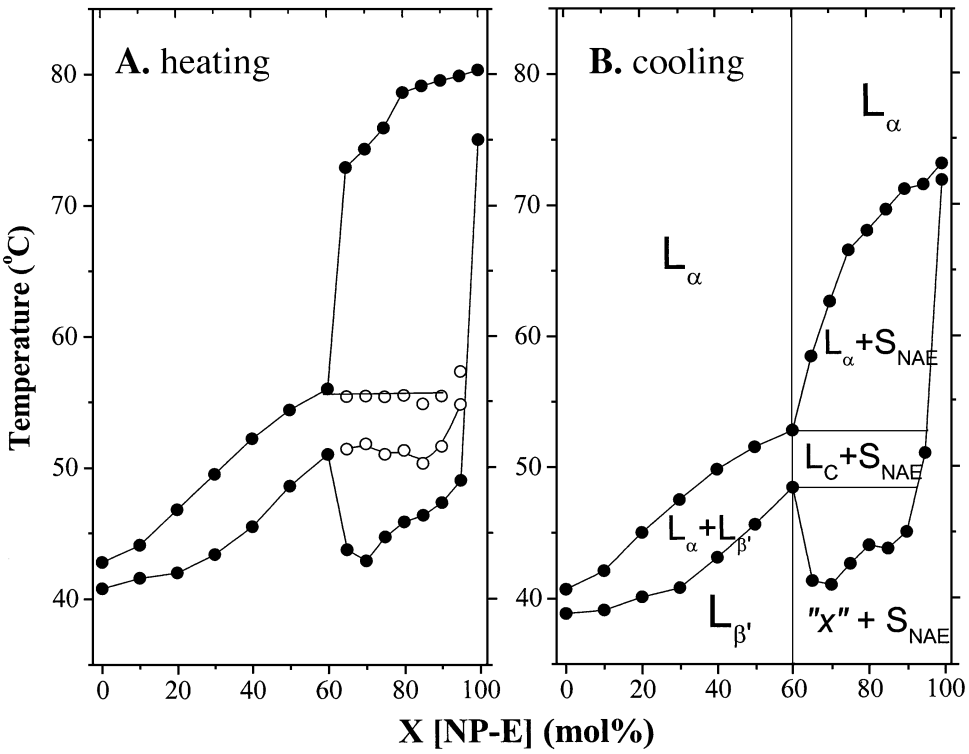

Fig. 3. Binary phase diagram of NP-E/DPPC mixtures dispersed in 10 mM HEPES, and 1 mM EDTA, pH 7.4, deduced from the phase boundaries established from the endothermic transitions observed in the heating scans (A), and the exothermic transitions observed in cooling scans (B), which are shown in Figs. 1 and 2, respectively. The *solidus* and *fluidus* points (solid symbols) were determined from the onset and completion of the change in the excess heat capacity, respectively. Open symbols in the range above 60 mol% NP-E represent the completion temperatures of the first and second peaks in the DSC scan. Phase designations are given in panel B. L_c is the gel phase of compound C and "x" is a putative second polymorph; S_{NAE} is solid NP-E (see Discussion).

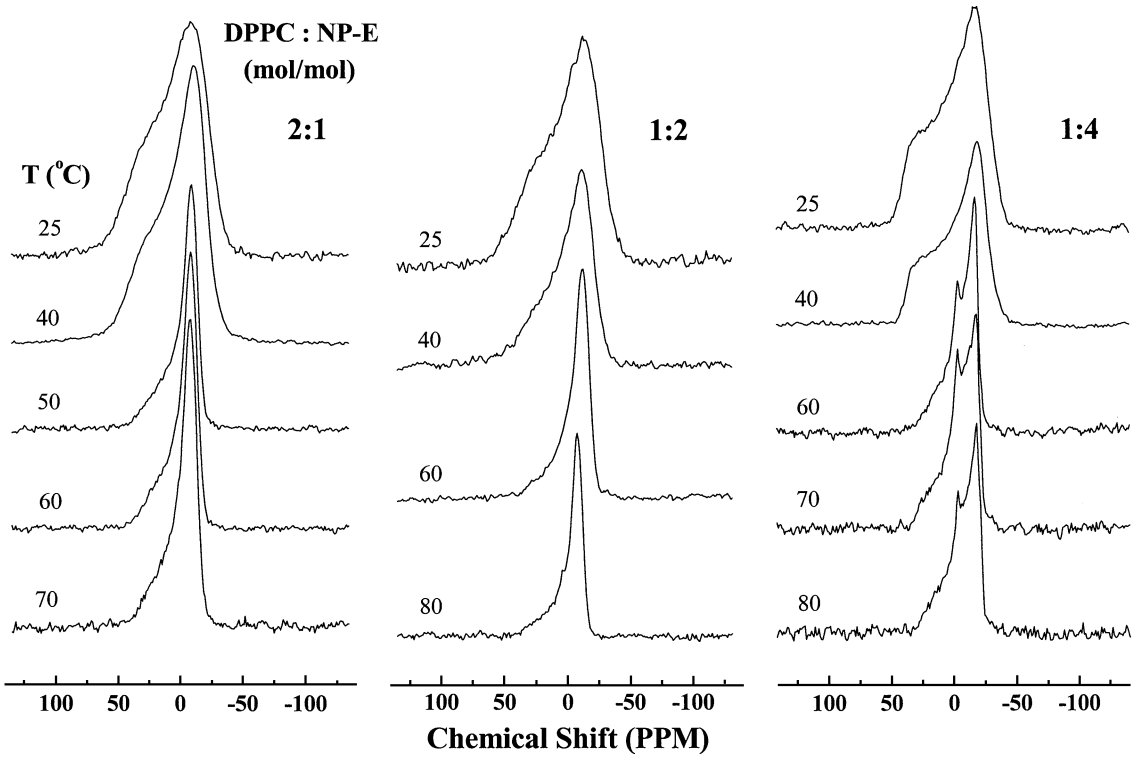

Fig. 4. Proton-dipolar decoupled 121.5 MHz ^{31}P-NMR spectra of NP-E/DPPC binary mixtures hydrated with 10 mM HEPES, 1 mM EDTA, pH 7.4. The lipid composition of the samples and the temperature at which each spectrum was recorded are indicated in the figure. Chemical shifts are referenced to external 85% phosphoric acid.

Table 1
Values of effective CSA, obtained from ^{31}P-NMR spectra of hydrated binary mixtures of DPPC and NP-E, recorded at different temperatures

DPPC/NP-E (mol/mol)	T (°C)	CSA (ppm)
2:1	25	− 71.2
	40	− 64.7
	50	− 49.0
	60	− 47.2
	70	− 48.8
1:2	25	− 71.0
	40	− 62.7
	60	− 50.8
	80	− 44.2
1:4	25	− 70.7
	40	− 66.3
	60	− 49.2
	70	− 50.2
	80	− 48.6

Buffer: 10 mM HEPES, 1 mM EDTA, pH 7.4.

to − 50.8 ppm, and are typical of a lamellar fluid phase. At 1:4 (mol/mol) DPPC/NP-E ratio, all the fluid-phase spectra are also sharp, axially anisotropic powder patterns with effective CSA values in the range of − 48.6 to − 50.2 ppm, but contain a small proportion of an isotropic component that is superimposed on the lamellar pattern, the content of which does not appear to change with temperature in the range studied.

3.4. Low-angle X-ray scattering

Fig. 5 gives the low-angle X-ray scattering profiles of DPPC, NP-E and their mixtures of different ratios. Data are shown for measurements performed at 20, 40, 60, and 80 °C, corresponding to the gel-phase region, the ripple-phase region of DPPC, a region corresponding to mixture of coexisting phases at higher NAPE contents, and the fluid-phase region, respectively.

In the gel-phase region, at 20 °C, two or three orders of diffraction are observed for pure DPPC as well as for the mixtures up to 60 mol% NP-E (see Fig. 5, panel A), although the second-order diffraction is broader and no third-order diffraction is seen with samples containing 50 and 60 mol% NP-E. At higher mole fractions of NP-E ($\geq$ 70%), an additional diffraction line is seen, indicating the coexistence of at least two different phases. Pure NP-E gave only a single reflection at all temperatures, over the scattering range studied. However, it most likely exists in the lamellar phase. Supporting evidence for this, although indirect, comes from single-crystal X-ray diffraction stud-

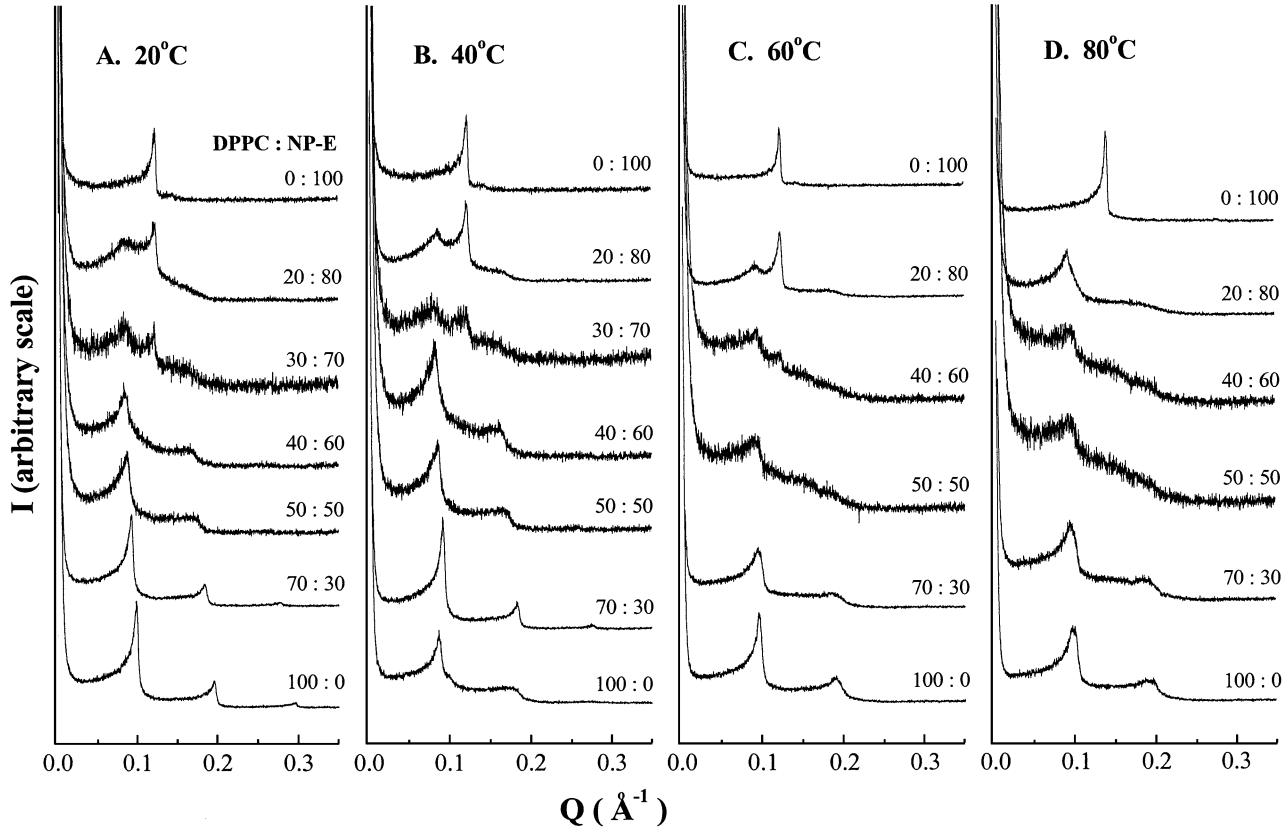

Fig. 5. Low-angle X-ray diffraction patterns of fully hydrated NP-E/DPPC binary mixtures at 20, 40, 60 and 80 °C. Buffer used for hydration is 10 mM HEPES, 1 mM EDTA, pH 7.4. The magnitude of the scattering vector, q ($Å^{-1}$) is $4\pi\sin\theta/\lambda$, where 2θ is the scattering angle. The molar composition of the lipid mixtures is indicated in the figure.

ies of NM-E and NS-E, both of which form a lamellar structure in the crystalline phase, with repeat spacing of 38.1 and 47.6 Å, respectively [17,21]. Because NP-E is homologous to these two compounds, with an intermediate chainlength, it is most likely that it would also adopt a lamellar bilayer-type structure in the solid state. At 20 °C, the hydrated sample of NP-E gives a single diffraction line, which corresponds to a repeat spacing of 50.7 Å. This is 12.6 Å more than the repeat spacing observed with dry NM-E and slightly larger (by 3.1 Å) than the repeat spacing of dry NS-E. Considering that NP-E contributes four additional CH_2 groups to the width of the bilayer as compared with NM-E, and that the diffraction data in this study are collected with a fully hydrated sample, the higher repeat spacing seen for NP-E seems consistent with a lamellar bilayer structure.

At 60 °C, the diffraction data arise from lamellar structures that consist of a single phase up to 50 mol% NP-E. The second-order reflection is more diffuse in this region, when compared with the diffraction patterns observed at 20 °C. At 60 mol% NP-E, an additional weak reflection is seen, the intensity of which increases as the content of NP-E is increased until, at 100 mol% NP-E, only the latter reflection is observed. These results suggest that between ca. 60 and 100 mol%, NP-E and its mixture with DPPC coexist.

At 80 °C, which corresponds to the fluid phase region at all the lipid compositions investigated, all samples up to 80 mol% NP-E give lamellar diffractions, whereas NP-E alone gives a single sharp reflection which corresponds to a repeat spacing of 44.9 Å. If NP-E alone forms a lamellar bilayer-type structure in the gel phase that undergoes a gel-to-liquid crystalline phase transition, then it would be expected that the fluid phase will have a lower repeat spacing because of *gauche* rotational isomers in the C–C single bonds of the acyl chain, which decrease the bilayer thickness. However, some compensating increase in thickness of the intervening water layers from an increased hydration in the fluid phase cannot be completely excluded.

Fig. 6 gives the dependence of the bilayer repeat spacing, d_{100}, on mole fraction (%) of NP-E, deduced from Fig. 5. In the gel phase at 20 °C (Fig. 6A), d_{100} increases steeply with increasing NP-E content (linear-regression slope = 0.179 ± 0.014 Å/mol%). At 40 °C (Fig. 6B), DPPC alone is in the intermediate P'_β-phase, for which the repeat spacing is greater than in the L'_β gel-phase. From 30 mol% NP-E onwards, the repeat spacing at 40 °C follows more closely that of the gel-phase at 20 °C, consistent with the disappearance of the pretransition at 20 mol% NP-E and above (see Fig. 1). At 60 °C (Fig. 6C), the repeat spacing increases until reaching the two-phase region of gel-fluid coexistence. In the fluid phase at 80 °C (Fig. 6D), the repeat spacing increases with increasing NP-E content, but to a much smaller degree than in the gel phase (linear-regression slope = 0.048 ± 0.015 Å/mol%).

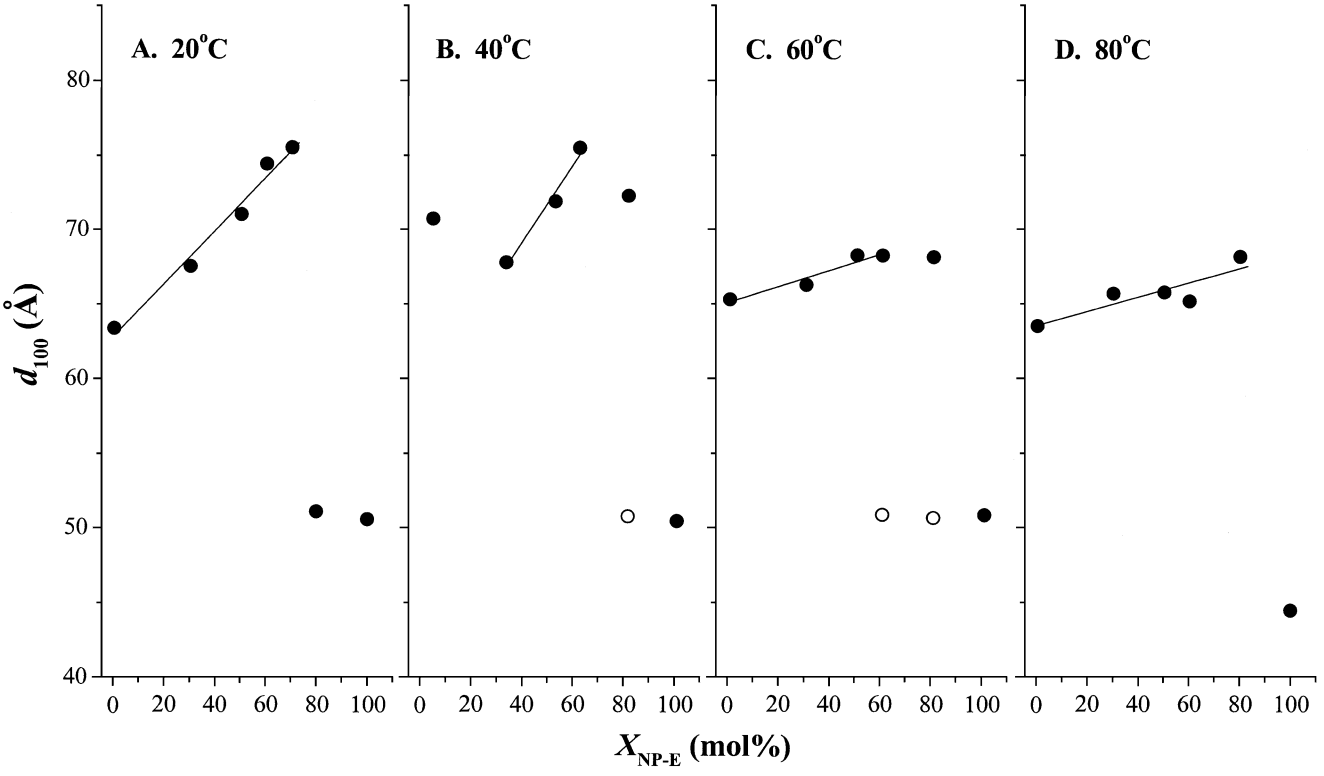

Fig. 6. Dependence of bilayer repeat spacing, d_{100}, on NP-E content in hydrated binary mixtures of DPPC/NP-E (10 mM HEPES, 1 mM EDTA, pH 7.4) at: (A) 20 °C (gel phase), (B) 40 °C (intermediate phase), (C) 60 °C (fluid/coexistence region), and (D) 80 °C (fluid phase). Sloping dotted lines are linear regressions.

4. Discussion

We first discuss the structure of the various phases of the hydrated DPPC-NP-E mixtures. Then we treat the phase coexistence and phase diagram of the binary mixtures. Finally, we consider the implications of the mixing properties of NP-E in lipid membranes.

4.1. Phase structures and component miscibility

Both low-angle X-ray diffraction and ^{31}P-NMR results indicate that the hydrated lipid mixtures possess a lamellar membrane structure at all compositions and temperatures investigated. ^{31}P-NMR reports only on the phases that contain DPPC, but provides no evidence for the existence of non-lamellar phases. The very small isotropic peak in the ^{31}P-NMR spectra of the DPPC/NP-E 1:4 mol/mol mixture in Fig. 4 most probably arises from small lamellar particles. Note that this peak first appears at the transition to the narrow lamellar powder pattern and, therefore, is associated with the L_α-phase.

The X-ray diffraction patterns are characteristic of a single lamellar structure at all temperatures for mixtures containing up to 50 mol% NP-E. The diffraction peaks become more diffuse with increasing NAPE content and increasing temperature in this range (see Fig. 5). This may indicate a decreasing coherence of the multilamellar structures or the formation of paucilamellar liposomal structures. Note, however, that the loss of sharp structure to the diffraction patterns does not arise from diffuse scattering of micellar disks because the CSA of the ^{31}P-NMR spectra (see Fig. 4) remains relatively large, even at NAPE contents above 50 mol% (Table 1).

The smooth and progressive increase in bilayer repeat spacing with increasing NP-E content up to 60 mol% at 20 °C indicates that the two components are miscible in the gel phase, throughout this composition range (Fig. 6A). From Fig. 6D, similar conclusions can be drawn, although less firmly, for the fluid phase at 80 °C. At the intermediate temperature of 60 °C, the repeat spacing remains constant from 50 to 80 mol% NP-E (Fig. 6B), in the L_α and L'_β phase-coexistence region. This value (d_{100} = 68.6 Å) corresponds to the fixed composition of the L'_β gel-phase in the coexistence region, as required by the Gibbs phase rule for a two-component system.

The increase of repeat distance with increasing NP-E content in the gel phase could be attributable to a decrease in tilt of the lipid chains and/or an increase in water-layer thickness. At 20 °C, in the L'_β-phase, the thickness of the DPPC bilayer is d_l = 47 Å and the molecular tilt is θ = 34° [22,23]. For an untilted structure, the bilayer thickness would therefore increase by Δd_l = + 10 Å. At 20 °C, the maximum increase in bilayer repeat distance observed here is comparable to this: $\Delta d_{100} \pm 12$ Å, for 70 mol% NP-E (Fig. 6A). A change in tilt is therefore a quantitatively feasible explanation for the increase in repeat spacing in the gel phase. In the fluid phase, the increase in bilayer repeat distance is much smaller and could readily be achieved by an increase in chain order, on addition of the higher-melting component. Again, changes in the degree of hydration also cannot be excluded in the fluid phase.

Above 60 mol% NP-E, a diffraction peak characteristic of NP-E alone appears superimposed on the scattering pattern from the mixture, both at 20 °C in the gel phase and at 60 °C in the phase coexistence region. This is a clear indication of gel-phase immiscibility at NP-E contents greater than 60 mol%. On the other hand, no additional diffraction peak appears superimposed on the scattering profiles at 80 °C, indicating that the two lipid components are miscible at all compositions in the fluid phase.

4.2. Binary phase diagram

In the composition range up to 60 mol% NP-E, the phase diagram is of the isomorphous type that is characteristic of miscibility of the two components in both the gel (L_β') and fluid (L_α) phases (see Fig. 3B). This is consistent with the ^{31}P-NMR and X-ray diffraction results that were discussed above. Although the endotherm for the DPPC/NP-E 60:40 mol/mol sample has a non-vanishing width, its shape is tending towards that for an isothermally melting compound. Possibly the phase diagram contains a non-congruent melting point and the NP-E/DPPC stoichiometry of the compound is somewhat greater than 3:2 mol/mol.

At NP-E contents above the stoichiometry of the NP-E/DPPC compound, the phase diagram is complex. The relatively high enthalpy of the low temperature section of the endotherms in Fig. 2 leads one to assign this to a chain-melting event, although a high-enthalpy solid-solid transition cannot entirely be excluded. With the first interpretation, the line with solid symbols at low temperature for $X_{NP\text{-}E}$>60 mol% should be a conventional *solidus* line. However, this line lies below the melting temperature of the NP-E/DPPC 3:2 mol/mol compound. It is therefore difficult to construct a phase diagram for mixtures of this compound with the higher-melting NPAE that is consistent with the Gibbs phase rule. The sudden appearance of the lower temperature section of the endotherm for mixtures with $X_{NP\text{-}E}$>60 mol% can possibly be explained by a second polymorphic form of NP-E (identified as "x" in Fig. 3B) that has a lower melting temperature. If this is the case, this polymorph must be stabilised by admixture with DPPC because the existence of such a possibly metastable state is not detected in the DSC scans of hydrated NP-E alone. This is also true if the second polymorphic form, "x", is instead involved in a solid-solid transition.

In the dry state, all even-chainlength NAEs with 14–20 C-atoms display two solid-solid phase transitions below the main chain-melting phase transition [15]. For dry NP-E these transitions occur at ca. 77 and 91 °C, however, and are not seen in the hydrated sample (Ref. [15]; Ramakrishnan and Swamy, unpublished observations). These observations

indicate the existence of several polymorphic forms in the solid phase for NAEs of different chainlengths. Indeed, recent studies on NS-E show that it can exist in at least three polymorphic forms [24].

Given that the low-temperature endotherms in the second region of the phase diagram at $X_{NP\text{-}E}$>60 mol% can be interpreted in terms of a second NP-E polymorph, interpretation of the rest of the phase diagram in this region is relatively straightforward. The horizontal, constant-temperature *solidus* line (shown as open circles and dotted line in Fig. 3) is indicative of solid-solid phase separation between the NP-E/DPPC compound (L_c) and NP-E alone (S_{NAE}). This is totally consistent with the appearance of a diffraction peak assigned to NP-E that is found in the gel phase for this region of the binary phase diagram, as was discussed above. The non-horizontal *fluidus* line at high temperature in turn indicates miscibility between the NP-E/DPPC complex and NP-E in the fluid phase. This again is consistent with the X-ray diffraction results already discussed.

It is of interest to compare the present phase diagram for NAEs with that established previously for mixtures of NAPE with phosphatidylcholine [25]. Whereas NP-E mixes well with DPPC at contents up to 60 mol%, it was found that *N*-myristoyl dimyristoylphosphatidylethanolamine mixes rather well with dimyristoyl phosphatidylcholine over the entire composition range, especially in the fluid phase. Because the chain-melting transitions of NAPEs are considerably lower than those of the corresponding single-chain NAEs, the NAPEs are therefore the more compatible with physiological fluid phospholipid bilayer membranes.

4.3. Implications

Interestingly, NP-E mixes well with phosphatidylcholine, a major mammalian membrane lipid species, at contents up to 60 mol%. Beyond this level, excess NP-E phase separates, except in the fluid phase, which is achieved only at high temperature for these lipid mixtures. The good mixing properties then imply that rather high local concentrations of NAEs can be tolerated without membrane disruption. Potentially, this feature can potentiate the effectivity of the antagonist in the immediate environment of the CB-2 receptor. Based on the present results for NP-E, it can be anticipated that the mixing properties of anandamide with membrane lipids may be even better, because of its reduced chain-melting temperature. This could further enhance the effectivity of this particular agonist for type-I cannabinoid receptors.

Although the major component, phosphatidylcholine, is not the only phospholipid species of mammalian cell membranes. In the future, it will be of interest to investigate the mixing properties of NAEs with other phospholipids, especially phosphatidylethanolamine. The latter phospholipids, relative to phosphatidylcholines, are well known to exhibit a preference for formation of non-lamellar fluid lipid phases. Based on the ability of single-chain amphiphiles to induce non-lamellar lipid phases, it is possible that NAEs are therefore deleterious to the long-term stability of cell membranes. For this reason, it is possible that NAEs are stored in membrane-compatible reservoirs of NAPEs [25] that are mobilised to NAEs only under conditions of membrane stress. Additionally, because both NAEs and phosphatidylethanolamines form intermolecular hydrogen bonds in the solid state [17,26], it would be interesting to investigate if their interaction may also be affected by this property.

Acknowledgements

This work was supported in part by a research grant from the Department of Science and Technology (India) to MJS. MRK was supported by a Senior Research Fellowship from the CSIR (India).

References

[1] H.H.O. Schmid, P.C. Schmid, V. Natarajan, *N*-acylated glycerophospholipids and their derivatives, Prog. Lipid Res. 29 (1990) 1–43.
[2] K.D. Chapman, Emerging physiological roles for *N*-acylphosphatidylethanolamine metabolism in plants: signal transduction and membrane protection, Chem. Phys. Lipids 108 (2000) 221–229.
[3] H.H.O. Schmid, P.C. Schmid, V. Natarajan, The *N*-acylation-phosphodiesterase pathway and cell signalling, Chem. Phys. Lipids 80 (1996) 133–142.
[4] T. Sugiura, S. Kondo, A. Sukagawa, T. Tonegawa, S. Nakane, A. Yamashita, Y. Ishima, K. Waku, Transacylase-mediated and phosphodiesterase-mediated synthesis of *N*-arachidonoylethanolamine, an endogenous cannbinoid-receptor ligand, in rat brain microsomes-comparison with synthesis from free arachidonic acid and ethanolamine, Eur. J. Biochem. 240 (1996) 53–62.
[5] W.A. Devane, L. Hanus, A. Breuer, R.G. Pertwee, L.A. Stevenson, G. Griffin, D. Gibson, A. Mandelbaum, A. Etinger, R. Mechoulam, Isolation and structure of a brain constituent that binds to the cannabinoid receptor, Science 258 (1992) 1946–1949.
[6] L. Facci, R. Daltoso, S. Romanello, A. Buriani, S.D. Skaper, A. Leon, Mast-cells express a peripheral cannbinoid receptor with differential sensitivity to anandamide and palmitoylethanolamide, Proc. Natl. Acad. Sci. U. S. A. 92 (1995) 3376–3380.
[7] H. Schuel, E. Goldstein, R. Mechoulam, A.M. Zimmerman, S. Zimmerman, Anandamide (arachidonylethanolamide), a brain cannbinoid receptor antagonist, reduces sperm fertilizing capacity in sea urchin eggs by inhibiting the acrosome reaction, Proc. Natl. Acad. Sci. U. S. A. 91 (1994) 7678–7682.
[8] L. Venance, D. Piomelli, J. Glowinski, C. Giaume, Inhibition by anandamide of gap-junctions and intracellular calcium signalling in striatal astrocytes, Nature 376 (1995) 590–594.
[9] M. Sugita, M. Williams, J.T. Dulaney, H.W. Moser, Ceramidase and ceramide synthesis in human kidney and cerebellum. Description of a new alkaline ceramidase, Biochim. Biophys. Acta 398 (1975) 125–131.
[10] K.D. Chapman, S. Tripathy, B. Venables, A.D. Desouza, *N*-Acylethanolamines—formation and molecular composition of a new class of plant lipids, Plant Physiol. 116 (1998) 1163–1168.
[11] D. Marsh, M.J. Swamy, Derivatised lipids in membranes. Physicochemical aspects of *N*-biotinyl phosphatidylethanolamines, *N*-acyl phosphatidylethanolamines and *N*-acyl ethanolamines, Chem. Phys. Lipids 105 (2000) 43–69.

[12] A. Ambrosini, E. Bertoli, P. Mariani, F. Tanfani, M. Wozniak, G. Zolese, *N*-Acylethanolamines as membrane topological stress compromising agents, Biochim. Biophys. Acta 1148 (1993) 351–355.
[13] A. Ambrosini, F. Tanfani, E. Bertoli, M. Wozniak, Z. Wypych, G. Zolese, Effect of *N*-acylethanolamines with different acyl chains on DPPC multilamellar liposomes, Chem. Phys. Lipids 65 (1993) 165–169.
[14] D.E. Epps, A.D. Cardin, The interactions of *N*-oleoylethanolamine with phospholipid bilayers, Biochim. Biophys. Acta 903 (1987) 533–541.
[15] M. Ramakrishnan, V. Sheeba, S.S. Komath, M.J. Swamy, Differential scanning calorimetric studies on the thermotropic phase transitions of dry and hydrated forms of *N*-acylethanolamines of even chainlengths, Biochim. Biophys. Acta 1329 (1997) 302–310.
[16] M. Ramakrishnan, M.J. Swamy, Differential scanning calorimetric studies on the thermotropic phase transitions of *N*-acylethanolamines of odd chainlengths, Chem. Phys. Lipids 94 (1998) 43–51.
[17] M. Ramakrishnan, M.J. Swamy, Molecular packing and intermolecular interactions in *N*-acylethanolamines: crystal structure of *N*-myristoylethanolamine, Biochim. Biophys. Acta 1418 (1999) 261–267.
[18] M.J. Swamy, B. Angerstein, D. Marsh, Differential scanning calorimetry of thermotropic phase transitions in vitaminylated lipids: aqueous dispersions of *N*-biotinyl phosphatidylethanolamines, Biophys. J. 66 (1994) 31–39.
[19] U. Würz, Small angle X-ray scattering of microemulsions, Prog. Colloid & Polym. Sci. 76 (1988) 153–158.
[20] D. Marsh, Handbook of Lipid Bilayers, CRC Press, Boca Raton, FL, 1990.
[21] B. Dahlén, I. Pascher, S. Sundell, Crystal structure of N-(2-hydroxyethyl)-octadecanamide, Acta Chem. Scand., Ser. A, Phys. & Inorg. Chem. 31 (1977) 313–320.
[22] M.J. Janiak, D.M. Small, G.G. Shipley, Nature of thermal pretransition of synthetic phospholipids: dimyristoyl- and dipalmitoyllecithin, Biochemistry 15 (1976) 4575–4580.
[23] M.J. Janiak, D.M. Small, G.G. Shipley, Temperature and compositional dependence of the structure of hydrated dimyristoyl lecithin, J. Biol. Chem. 254 (1979) 6068–6078.
[24] J. Wouters, S. Vandevoorde, C. Culot, F. Docquir, D.M. Lambert, Polymorphism of *N*-stearoylethanolamine: differential scanning calorimetric, vibrational spectroscopic (FTIR), and crystallogrpaphic studies, Chem. Phys. Lipids 119 (2002) 13–21.
[25] M. Ramakrishnan, D. Marsh, M.J. Swamy, Interaction of *N*-myristoyldimyristoylphosphatidylethanolamine with dimyristoylphosphatidylcholine investigated by differential scanning calorimetry: binary phase diagram, Biochim. Biophys. Acta 1512 (2001) 22–26.
[26] M. Elder, P. Hitchcock, R. Mason, G.G. Shipley, A refinement analysis of the crystallography of the phospholipid, 1,2-dilauroyl-DL-phosphatidylethanolamine, and some remarks on lipid-lipid and lipid-protein interactions, Proc. R. Soc. Lond., A 354 (1977) 157–170.